Neurobiology of Aging 83 (2019) 54–62

Contents lists available at ScienceDirect

Neurobiology of Aging

journal homepage: www.elsevier.com/locate/neuaging

Tracking white matter degeneration in asymptomatic and symptomatic *MAPT* mutation carriers

Qin Chen [a,b], Bradley F. Boeve [c], Christopher G. Schwarz [b], Robert Reid [b], Nirubol Tosakulwong [d], Timothy G. Lesnick [d], Jessica Bove [e], Patrick Brannelly [f], Danielle Brushaber [d], Giovanni Coppola [g], Christina Dheel [c], Bradford C. Dickerson [h], Susan Dickinson [i], Kelley Faber [j], Julie Fields [k], Jamie Fong [l], Tatiana Foroud [j], Leah Forsberg [c], Ralitza H. Gavrilova [c], Debra Gearhart [c], Nupur Ghoshal [m], Jill Goldman [n], Jonathan Graff-Radford [c], Neill R. Graff-Radford [o], Murray Grossman [e], Dana Haley [o], Hilary W. Heuer [l], Ging-Yuek R. Hsiung [p], Edward Huey [n], David J. Irwin [e], Clifford R. Jack [b], David T. Jones [c], Lynne Jones [q], Anna M. Karydas [l], David S. Knopman [c], John Kornak [r], Joel Kramer [l], Walter Kremers [d], Walter A. Kukull [s], Maria Lapid [k], Diane Lucente [h], Codrin Lungu [t], Ian R.A. Mackenzie [u], Masood Manoochehri [n], Scott McGinnis [h], Bruce L. Miller [l], Rodney Pearlman [v], Leonard Petrucelli [w], Madeline Potter [j], Rosa Rademakers [w], Eliana M. Ramos [g], Katherine P. Rankin [l], Katya Rascovsky [e], Pheth Sengdy [p], Leslie Shaw [x], Jeremy Syrjanen [d], Nadine Tatton [i], Joanne Taylor [l], Arthur W. Toga [y], John Trojanowski [x], Sandra Weintraub [z], Bonnie Wong [h], Adam L. Boxer [l], Howie Rosen [l], Zbigniew Wszolek [o], Kejal Kantarci [b,*], on behalf of the LEFFTDS Consortium

[a] *Department of Neurology, West China Hospital of Sichuan University, Chengdu, Sichuan, China*
[b] *Department of Radiology, Mayo Clinic, Rochester, MN, USA*
[c] *Department of Neurology, Mayo Clinic, Rochester, MN, USA*
[d] *Department of Health Sciences Research, Mayo Clinic, Rochester, MN, USA*
[e] *Department of Neurology, Perelman School of Medicine, University of Pennsylvania, Philadelphia, PA, USA*
[f] *Tau Consortium, Rainwater Charitable Foundation, Fort Worth, TX, USA*
[g] *Department of Psychiatry and Biobehavioral Sciences, University of California, Los Angeles, Los Angeles, CA, USA*
[h] *Department of Neurology, Frontotemporal Disorders Unit, Massachusetts General Hospital, Harvard University, Boston, MA, USA*
[i] *Association for Frontotemporal Degeneration, Radnor, PA, USA*
[j] *National Cell Repository for Alzheimer's Disease (NCRAD), Indiana University, Indianapolis, IN, USA*
[k] *Department of Psychiatry and Psychology, Mayo Clinic, Rochester, MN, USA*
[l] *Department of Neurology, Memory and Aging Center, University of California, San Francisco, San Francisco, CA, USA*
[m] *Departments of Neurology and Psychiatry, Washington University School of Medicine, St. Louis, MO, USA*
[n] *Department of Neurology, Columbia University, New York, NY, USA*
[o] *Department of Neurology, Mayo Clinic, Jacksonville, FL, USA*
[p] *Division of Neurology, Department of Medicine, University of British Columbia, Vancouver, British Columbia, Canada*
[q] *Department of Radiology, Washington University School of Medicine, Washington University, St. Louis, MO, USA*
[r] *Department of Epidemiology and Biostatistics, University of California, San Francisco, San Francisco, CA, USA*
[s] *National Alzheimer Coordinating Center (NACC), University of Washington, Seattle, WA, USA*
[t] *National Institute of Neurological Disorders and Stroke (NINDS), Bethesda, MD, USA*
[u] *Department of Pathology and Laboratory Medicine, University of British Columbia, Vancouver, British Columbia, Canada*
[v] *Bluefield Project, San Francisco, CA, USA*
[w] *Department of Neurosciences, Mayo Clinic, Jacksonville, FL, USA*
[x] *Department of Pathology and Laboratory Medicine, Perelman School of Medicine, University of Pennsylvania, Philadelphia, PA, USA*
[y] *Departments of Ophthalmology, Neurology, Psychiatry and the Behavioral Sciences, Laboratory of Neuroimaging (LONI), USC, Los Angeles, CA, USA*
[z] *Department of Neurology, Feinberg School of Medicine, Northwestern University, Chicago, IL, USA*

* Corresponding author at: Department of Radiology, Mayo Clinic, 200 First Street SW, Rochester, MN 55905, USA. Tel.: 507-284 9770; fax: 507-284 9778.
E-mail address: kantarci.kejal@mayo.edu (K. Kantarci).

0197-4580/$ – see front matter
https://doi.org/10.1016/j.neurobiolaging.2019.08.011

ARTICLE INFO

Article history:
Received 14 February 2019
Received in revised form 7 August 2019
Accepted 11 August 2019
Available online 15 August 2019

Keywords:
Diffusion tensor image
MAPT
Asymptomatic
Frontotemporal dementia
Longitudinal

ABSTRACT

Our aim was to investigate the patterns and trajectories of white matter (WM) diffusion abnormalities in microtubule-associated protein tau (*MAPT*) mutations carriers. We studied 22 *MAPT* mutation carriers (12 asymptomatic, 10 symptomatic) and 20 noncarriers from 8 families, who underwent diffusion tensor imaging (DTI) and a subset (10 asymptomatic, 6 symptomatic *MAPT* mutation carriers, and 10 noncarriers) were followed annually (median = 4 years). Cross-sectional and longitudinal changes in mean diffusivity (MD) and fractional anisotropy were analyzed. Asymptomatic *MAPT* mutation carriers had higher MD in entorhinal WM, which propagated to the limbic tracts and frontotemporal projections in the symptomatic stage compared with noncarriers. Reduced fractional anisotropy and increased MD in the entorhinal WM were associated with the proximity to estimated and actual age of symptom onset. The annualized change of entorhinal MD on serial DTI was accelerated in *MAPT* mutation carriers compared with noncarriers. Entorhinal WM diffusion abnormalities precede the symptom onset and track with disease progression in *MAPT* mutation carriers. Our cross-sectional and longitudinal data showed a potential clinical utility for DTI to track neurodegenerative disease progression for *MAPT* mutation carriers in clinical trials.

1. Introduction

Frontotemporal lobar degeneration (FTLD) is a progressive neurodegenerative disease associated with behavioral and language disorders, executive dysfunction, and impaired social cognition (Bang et al., 2015). About 30%–50% FTLD patients have an autosomal dominant pattern of inheritance (Rohrer and Warren, 2011), with many showing mutations in the microtubule associated protein tau (*MAPT*) gene (Spillantini et al., 1998). Mutations in *MAPT* result in filamentous accumulation of hyperphosphorylated tau in neurons and glia leading to neurodegeneration, atrophy, and white matter (WM) microstructure alterations years before the onset of clinical symptoms (Bunker et al., 2006; Cash et al., 2018; Dopper et al., 2014; Ingram and Spillantini, 2002; Kantarci et al., 2010). Families with *MAPT* mutations provide a unique opportunity to investigate early disease-burden brain changes and identify biomarkers for tracking disease progression in the context of potential disease-modifying therapies.

Diffusion tensor imaging (DTI) is sensitive to the WM microstructure alterations, such as loss of myelin and axonal membranes. Loss of WM microstructural integrity on DTI was associated with cerebrospinal fluid biomarkers of tau protein and Braak staging of the neurofibrillary tangle tau pathology in Alzheimer's disease (Bendlin et al., 2012; Kantarci et al., 2017). Damage to WM caused by tau pathology is a frequent observation in postmortem examinations of genetic and sporadic cases of patients with FTLD (Kovacs et al., 2008; Larsson et al., 2000; Sima et al., 1996) and in animals expressing tau mutations (Gotz et al., 2001; Lin et al., 2003). Recently, focal myelin injury was identified as the first manifestation of tauopathy in a tauP301L mouse model (Jackson et al., 2018). Despite the growing literature of DTI findings in patients with FTLD and in asymptomatic carriers of the granulin (*GRN)* (Pievani et al., 2014) and chromosome 9 open reading frame 72 (*C9orf72*) mutations (Bertrand et al., 2018), few studies have demonstrated microstructural WM changes in asymptomatic *MAPT* mutation carriers (Dopper et al., 2014; Jiskoot et al., 2018, 2019; Panman et al., 2019). We hypothesized that DTI measures of WM microstructure occur early in asymptomatic *MAPT* mutation carriers and the trajectory of DTI changes are associated with the disease progression during longitudinal follow-up.

Our objectives were 1) to determine the DTI abnormalities across all WM regions of interest (ROIs) to distinguishing asymptomatic and symptomatic *MAPT* mutation carriers from noncarriers; 2) to estimate the relationship between diffusion abnormalities and proximity to symptom onset in *MAPT* mutation carriers; 3) to compare the trajectory of DTI changes on serial DTI in *MAPT* mutation carriers compared with noncarriers.

2. Methods

2.1. Participants

Individuals in this study were participants enrolled in the Mayo Alzheimer's Disease Research Center and Longitudinal Evaluation of Familial Frontotemporal Dementia Subjects study at the Mayo Clinic site. Longitudinal Evaluation of Familial Frontotemporal Dementia Subjects is a national multisite study longitudinally investigating the biomarkers of disease progression in familial FTLD mutation carriers. The present study included participants who had screened positive for a mutation in *MAPT* and who were followed at the Mayo Clinic. A cohort of 22 *MAPT* mutation carriers from 8 individual families was enrolled at the baseline. Noncarriers from healthy first-degree relatives of the patients were recruited as a control group after DNA screening (n = 20). Participants were followed prospectively with annual clinical evaluation at the time of magnetic resonance imaging (MRI) examination, including a medical history review, mental status examination, a neurological examination, and a neuropsychological examination. The behavioral neurologist (BB, JGR, NGR, DJ, or DK) who examined all of the participants was blinded to the mutation status. None of the participants fulfilled the exclusion criteria.

Inclusion criteria include the following: 1) participants are eligible for enrollment if they are members of families with a known mutation in *MAPT* and are aged 18 years or older, and preferably above age 30 years; 2) the predominant phenotype in the kindred should be cognitive/behavioral (i.e., kindreds in whom behavioral variant frontotemporal dementia (bvFTD) or primary progressive aphasia is the predominant clinical phenotype among affected relatives is favored over parkinsonism or ALS, although all phenotypes are eligible for enrollment); 3) a reliable informant who personally speaks with or sees that participant at least weekly; 4) participant is sufficiently fluent in English to complete all measures, 5) willing and able to consent to the protocol and undergo yearly evaluations, 6) willing and able to undergo neuropsychological testing (at least at the baseline visit), and 7) no contraindication to MRI.

Exclusion criteria include 1) absence of a known mutation in *MAPT* in the participant or family; 2) presence of a structural brain lesion (e.g., tumor, cortical infarct); 3) presence of another neurologic disorder which could impact findings (e.g., multiple sclerosis);

Table 1
Participant characteristics at the baseline

	Noncarrier (N = 20)	Asymptomatic (N = 12)	Symptomatic (N = 10)	*p*-value
No. female (%)	9 (45%)	8 (67%)	4 (40%)	0.50
Education, y	14.4 (2.6)	15.7 (2.1)	14.3 (2.5)	0.31
Age at DTI scan, y	49.1 (15.3)	36.5 (7.3)	54.2 (11.7)	<0.001[a]
MMSE	29.4 (1.4)	29.8 (0.4)	20.2 (11.3)	<0.001[b]
CDR plus NACC FTLD SOB	0.2 (0.6)	0.1 (0.2)	11.6 (7.8)	<0.001[b]
DRS total MOANS	11.6 (2.6)	14.0 (1.8)	5.2 (2.9)	<0.001[b]
No. of longitudinal subcohort (%)	10 (50%)	10 (83%)	6 (60%)	0.58
No. DTI scans	2.5 (0.7)	3.2 (1.1)	4.3 (1.8)	0.08[c]
Follow-up, y	4.0 (0.7)	3.9 (0.6)	3.4 (0.8)	0.12

Data shown are n (%) or median (range).
p-values are from Fisher's exact test or Kruskal-Wallis rank sum Test followed by Wilcoxon rank sum test.
Key: DTI, diffusion tensor image; MMSE, Mini-Mental State Examinations; CDR, Clinical Dementia Rating; NACC, National Alzheimer Coordinating Center; FTLD, frontotemporal lobar degeneration; DRS, dementia rating scale; MOANS, Mayo's Older Americans Normative Studies.
[a] Asymptomatic is statistically different from other groups.
[b] Symptomatic is statistically different from other groups.
[c] All groups are statistically different from each other.

4) unwillingness to return for follow-up yearly; 5) unwillingness to undergo neuropsychological testing and MRI; and 6) no reliable informant.

2.2. Baseline characteristics

Participants' demographic and clinical characteristics are shown in Table 1. Of the 22 *MAPT* mutation carriers at the baseline, 12 participants had no clinical symptoms and a CDR Dementia Staging Instrument plus NACC FTLD Behavior and Language Domains sum of boxes (CDR plus NACC FTLD-SB) (Knopman et al., 2008) of 0, which we refer to as asymptomatic *MAPT* mutation carriers. The remaining *MAPT* mutation carriers (n = 10) were symptomatic and had a mean CDR plus NACC FTLD-SB score of 11.6 including 5 patients diagnosed with bvFTD, 4 with bvFTD and parkinsonism, and 1 with mild cognitive impairment behavior. The clinical status was based on the key ratings for the assessment team, including the scale, neuropsychological data, the consensus clinical diagnostic assessment (Rascovsky et al., 2011), and the confidence rating. The mutations identified in these symptomatic *MAPT* mutation carriers were as follows: V337M (n = 3), P301L (n = 3), S305N (n = 2), Q336H (n = 1) and N279K mutations (n = 1).

Estimated age of symptom onset was calculated as the median age at symptom onset among all symptomatic carriers in each family/mutation type based on the clinical history on these families.

2.3. Longitudinal cohort

A subset of participants (n = 29) received at least 2 DTI scans with a total of 100 DTI scans. After quality control measures, we had to exclude 3 symptomatic *MAPT* mutation carriers and 17 DTI scans (8 with a head motion artifact, 7 with failure of image analysis, and 2 with incomplete brain coverage) from further analyses. Finally, 26 participants (10 asymptomatic, 6 symptomatic *MAPT* mutation carriers, and 10 noncarriers) with a total of 83 DTI scans were included in the longitudinal analysis (Supplemental Table 1).

All symptomatic *MAPT* mutation carriers described in this report have undergone clinical genetic testing and therefore they and/or their proxies are aware of their mutation status. Most of the asymptomatic mutation carriers included in present study had not undergone clinical genetic testing, and therefore they are not aware of their mutation status. Personal identifiers have been excluded to maintain confidentiality. Informed consent, which was approved by the Mayo Institutional Review Board, was obtained from all participants before participation in the studies.

2.4. MRI and DTI scanning

All MRI studies were performed at 3T with an 8-channel phased array head coil (GE Healthcare, Milwaukee, WI, USA). A 3D high-resolution T1-weighted magnetization-prepared rapid gradient echo acquisition was performed with repetition time/echo time/inversion time = 2300/3/900 msec, flip angle 8°, voxel resolution 1.2 × 1 × 1 mm. A single-shot echo-planar DTI pulse sequence was performed in the axial plane, with repetition time 10,200 msec, in-plane matrix 128 × 128, field of view 35 cm. The DTI volumes consisted of 41 diffusion-encoding gradient directions and 5 volumes of nondiffusion T2-weighted images. Parallel imaging with a SENSE factor of 2 was used. The slice thickness was 2.7 mm, corresponding to 2.7-mm isotropic resolution.

2.5. Image analysis

DTI images were initially corrected for subject motion and residual eddy current distortion by affine-registering each volume to the first image volume with no diffusion weighting. Images were skull stripped using a previously published method (Reid et al., 2018). Diffusion tensors were fit for extracted voxels using weighted linear least squares optimization, and maps of fractional anisotropy (FA) and mean diffusivity (MD) images were calculated from the eigenvalues of the tensors using Dipy (Garyfallidis et al., 2014). We performed an ROI-based analysis using the John's Hopkins University (JHU) single-subject "Eve" DTI atlas (Oishi et al., 2008). Advanced normalization tools—symmetric normalization (ANTs-SyN) version 1.9.y (Avants et al., 2011) was used to nonlinearly register the JHU FA template to each subject's FA image and transform the atlas. We then measured the mean DTI scalar values within each atlas region. Regional values were averaged across the left/right hemispheres and gray matter regions were omitted, leaving 43 WM ROIs for analysis (Supplemental Table 2). The results were displayed on a rendered transparent brain for visualization using MRIcroGL (http://www.mccauslandcenter.sc.edu/mricrogl/).

2.6. Genetic analysis

Analysis of *MAPT* exons 1, 7, and 9–13 was performed using primers and conditions that were previously reported (Hutton et al., 1998). PCR amplicons were purified using the Multiscreen system (Millipore, Billerica, MA, USA) and then sequenced in both directions using Big Dye chemistry following the manufacturer's protocol (Applied Biosystems, Foster City, CA, USA). Sequence products were purified using the Montage system (Millipore)

before being run on an Applied Biosystem 3730 DNA Analyzer. Sequence data were analyzed using either SeqScape (Applied Biosystem) or Sequencher software (Gene Codes, Ann Arbor, MI, USA).

2.7. Statistical analysis

Baseline characteristics were described with means, standard deviations, counts, and proportions. Baseline characteristics were compared among asymptomatic, symptomatic *MAPT* mutation carriers, and noncarriers using logistic mixed effect models for sex and linear mixed effect models for the other variables. These models were adjusted for age at DTI where appropriate, and accounted for within-family correlations. Tukey contrasts based on the mixed models were used for pairwise comparisons for continuous variables.

The weighted median of the tract-based MD and FA values derived from WM JHU atlas ROIs combining the right and left hemispheric regions were determined. Because age influences DTI measures, we used the data from the noncarriers to estimate the age effects on DTI measures and adjusted the MD and FA values in the *MAPT* mutation carriers for age. Predicted probabilities accounting for family mutation was used to calculate the estimates area under the receiver operating characteristics curves (AUROC) for each ROI to distinguish the *MAPT* mutation carriers from noncarriers. The DTI values from the asymptomatic and symptomatic *MAPT* carriers were compared with noncarriers, and ranked according to AUROC values. Because we were conducting comparisons in 43 different ROIs, we adjusted for multiple comparisons to control the familywise error rate. Significant after correction for multiple comparisons were displayed on a rendered single-participant transparent brain for visualization (Fig. 1).

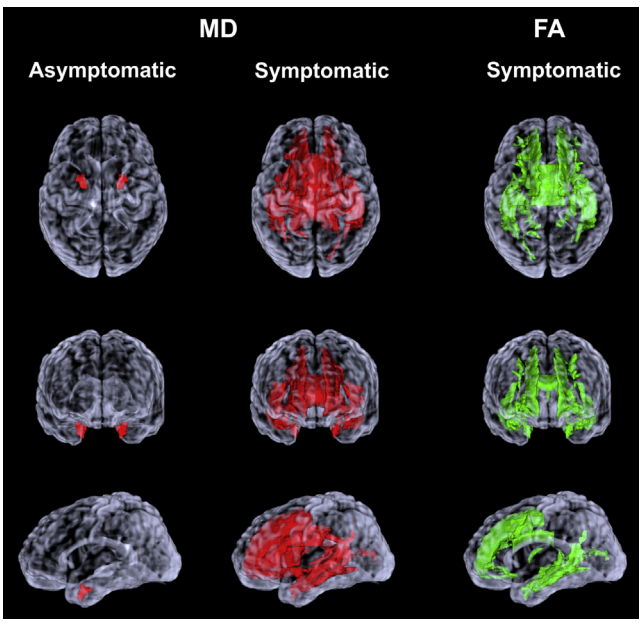

Fig. 1. Region of interest analysis. WM regions of interest with increased MD in asymptomatic and symptomatic *MAPT* mutation carriers compared with noncarriers are displayed on a rendered transparent brain from a single participant (colored in red). WM regions of interest with reduced FA in symptomatic *MAPT* mutation carriers compared with noncarriers are colored in green. MD and FA values from regions of interest that distinguished the *MAPT* mutation carriers from noncarriers with an area under the receiver operating characteristic curve (AUROC) of $p < 0.05$ after adjusting for age and correcting for multiple comparisons. Abbreviations: FA, fractional anisotropy; *MAPT*, microtubule-associated protein tau; MD, mean diffusivity; WM, white matter. (For interpretation of the references to color in this figure legend, the reader is referred to the Web version of this article.)

The association between DTI values and time to expected age of onset and time past age of onset was tested using multiple linear regression analysis after adjusting for age. We tested interactions between time from symptom onset and groups in FA and MD in these models. A significant interaction would produce a change in the estimated slopes at the time of symptom onset.

To assess the longitudinal DTI abnormalities, we modeled DTI metrics from each individual time-point to estimate annualized rate of change in FA and MD. The annual changes in FA and MD over time were modeled to compare *MAPT* mutation carriers to noncarriers using linear mixed-effect models with random subject-specific intercepts and slopes, while accounting for within-family correlations. Owing to the small sample size of this group, we only analyzed regions that showed abnormal FA and MD values in the cross-sectional analysis in asymptomatic *MAPT* mutation carriers. We coded group (noncarriers, asymptomatic, or symptomatic) using dummy variables with noncarrier as the reference, and included two-way interactions for group × age at MRI scan.

3. Results

3.1. Characteristics of participants

Characteristics of participants in each group at the baseline are listed in Table 1. The *MAPT* mutation carriers and noncarriers did not differ in sex and level of education. The asymptomatic *MAPT* mutation carriers were significantly younger than symptomatic *MAPT* mutation carriers ($p < 0.001$) and noncarriers ($p = 0.03$). Therefore, all cross-sectional analyses on the DTI data were adjusted for age. As expected, symptomatic *MAPT* mutation carriers scored lower on the Mini-Mental State Examinations and had a higher score (i.e., more abnormal) on CDR plus NACC FTLD-SB than asymptomatic *MAPT* mutation carriers and noncarriers. In the longitudinal cohort, there were no differences in sex and level of education across 3 groups at the baseline; however, asymptomatic *MAPT* mutation carriers were younger than symptomatic *MAPT* mutation carriers ($p = 0.01$) and noncarriers ($p = 0.02$). The symptomatic *MAPT* mutation carriers had more DTI scans compared with noncarriers ($p = 0.03$), but there were no differences in follow-up time range among the 3 groups.

The median follow-up time was 4 years (range 1–5 years) for the asymptomatic *MAPT* mutation carriers, 3 years (range 2–4 years) for the symptomatic *MAPT* mutation carriers, and 4 years (range 2–5 years) for the noncarriers. There were 2 asymptomatic *MAPT* mutation carriers from the same family, with a N279K mutation, who transitioned from asymptomatic to symptomatic during follow-up. Both patients were diagnosed with mild cognitive impairment behavior according to the consensus criteria (Rascovsky et al., 2011).

3.2. Cross-sectional regional WM change

On average, there were no differences in left and right hemispheric WM tract FA values ($p = 0.18$), but the hemispheric MD was higher on the right than the left side ($p = 0.01$) in *MAPT* mutation carriers at the baseline. However, for practicality, we averaged right and left hemispheric DTI measurements. We ranked the 43 JHU-atlas ROIs according to the AUROC for distinguishing asymptomatic and symptomatic *MAPT* mutation carriers from noncarriers using baseline MD and FA values (Supplemental Fig. 1A and B).

3.2.1. *Asymptomatic* MAPT *mutation carriers versus noncarriers*

The MD values in the entorhinal WM were higher in the asymptomatic *MAPT* mutation carriers compared with the noncarriers after adjusting for age and correcting for multiple

comparisons ($p = 0.01$). There were no differences in FA values from any of the ROIs between asymptomatic *MAPT* mutation carriers and noncarriers (Fig. 1).

3.2.2. Symptomatic MAPT *mutation carriers versus noncarriers*

In symptomatic *MAPT* mutation carriers, MD was higher in a number of ROIs compared with noncarriers after applying FDR correction for multiple comparisons, including the WM connections of the limbic system network (entorhinal WM, fornix, uncinate fasciculus, cingulum, corpus callosum), as well as the subcortical WM in the temporal lobe (inferior and superior temporal WM, middle temporal WM) and frontal lobe (superior frontal WM, gyrus rectus WM, medial and lateral fronto-orbital WM), and the connections of frontal and occipital lobes (inferior fronto-occipital fasciculus, sagittal stratum, precuneus, and cuneus WM) and the corticospinal tracts (anterior and superior corona radiata, internal capsule anterior limb). The number of ROIs with lower FA in symptomatic *MAPT* mutation carriers compared with noncarriers was similar but lower than the number of ROIs showing increased MD, which also included the limbic system network (fornix, entorhinal WM, cingulum, corpus callosum), the subcortical WM in the temporal lobe (middle and inferior temporal WM) and the frontal lobe (superior and middle frontal WM, middle and lateral fronto-orbital WM), and the connections of frontal and occipital lobes (sagittal stratum, precuneus, and cuneus WM) (Fig. 1).

3.3. Relationship with proximity to symptom onset

Median age at symptom onset in the 8 families ranged from 30 to 67 years at the baseline. The median of estimated proximity to symptom onset was −6 years (range −24 to 0 years) in asymptomatic *MAPT* mutation carriers, and the median of actual proximity to symptom onset was 8 years (range 1–27 years) in symptomatic *MAPT* mutation carriers (Supplemental Table 3).

3.3.1. MAPT *mutation carriers*

Because we found DTI alterations only in the entorhinal WM ROI in asymptomatic *MAPT* carriers, an association between the estimated or actual proximity to symptom onset and DTI metrics from entorhinal WM was analyzed (Fig. 2). The FA declined as the ages of *MAPT* mutation carriers approached the estimated age of symptom onset and passed actual age at the symptom onset ($p < 0.001$).

3.3.2. Symptomatic versus asymptomatic MAPT *mutation carriers*

There were no differences between the slopes of entorhinal WM FA in asymptomatic and symptomatic *MAPT* mutation carriers on multiple regression analysis ($p = 0.23$). On the contrary, the slope in symptomatic *MAPT* mutation carriers was significantly steeper than in asymptomatic carriers ($p = 0.02$), and MD increased as the ages of *MAPT* mutation carriers passed the actual age at the symptom onset ($p = 0.004$) (Table 2).

3.4. Longitudinal entorhinal WM change

Because we found DTI alterations only in the entorhinal WM ROI in asymptomatic *MAPT* mutation carriers, we compared groupwise rates of DTI metrics in entorhinal WM between the all *MAPT* mutation carriers and noncarriers due to the small sample size. The results of linear mixed-effects models are summarized in Table 3. Fig. 3 shows that the trajectories of MD in entorhinal WM increased faster with aging in *MAPT* mutation carriers compared with noncarriers in the mixed-effect models ($p = 0.002$). The difference in the decline of FA in the entorhinal WM between *MAPT* mutation carriers and noncarriers did not reach statistical significance ($p = 0.06$).

Table 4 shows the groupwise rates of DTI metrics in entorhinal WM among 3 groups. The trajectories of MD in entorhinal WM increased faster with aging in symptomatic *MAPT* mutation carriers compared with noncarriers in the mixed-effect models ($p < 0.001$). The difference in the rates of annual change MD in the entorhinal WM between asymptomatic *MAPT* mutation carriers and noncarriers did not reach statistical significance ($p = 0.18$). No difference of the rates of annual change FA in entorhinal WM is observed in asymptomatic and symptomatic *MAPT* mutation carriers compared with noncarriers.

4. Discussion

In this study, we examined the cross-sectional and longitudinal DTI abnormalities in asymptomatic and symptomatic *MAPT* mutation carriers. Our main findings are 1) elevated MD in the entorhinal

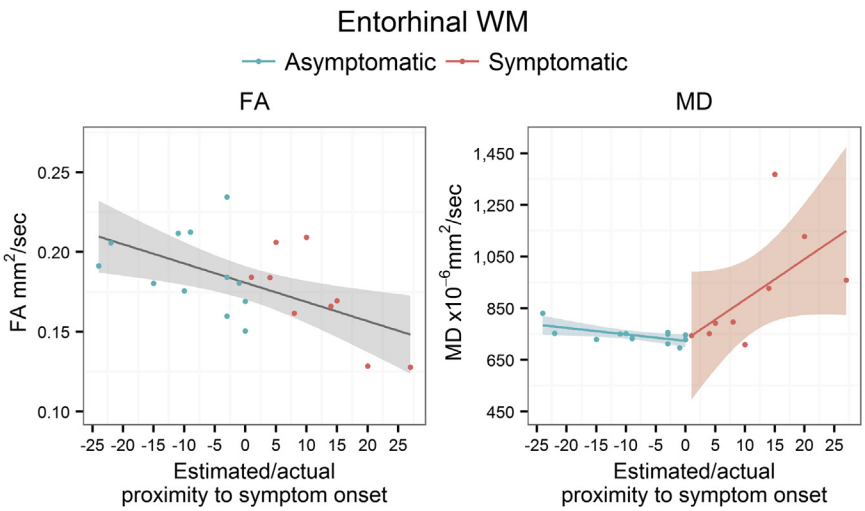

Fig. 2. Plots of age-adjusted FA and MD from entorhinal WM and the estimated or actual proximity to symptom onset. In the horizontal axis, 0 indicates the estimated age of symptom onset for asymptomatic *MAPT* mutation carriers based on the median age at the symptom onset in symptomatic *MAPT* mutation carriers from the same family. 0 indicates the age at actual symptom onset in symptomatic *MAPT* mutation carriers. Abbreviations: FA, fractional anisotropy; MD, mean diffusivity; *MAPT*, microtubule-associated protein tau; WM, white matter.

Table 2
Entorhinal WM multiple regression analysis testing the relationship between entorhinal FA and MD values with estimate or actual proximity to symptom onset in *MAPT* mutation carriers

	FA			MD		
	Est (95% CI)	*p*	R^2	Est (95% CI)	*p*	R^2
Intercept	0.15 (0.13, 0.17)	<0.001	0.48	8165 (7103, 9226)	<0.001	0.60
Time from onset	−0.002 (−0.0035, −0.0007)	0.006		−8 (−100, 83)	0.85	
Symptomatic	0.015 (−0.02, 0.05)	0.40		177 (−1663, 2016)	0.84	
Symptomatic × time from onset				176 (34, 317)	0.02	

For FA, model includes only time from onset and group (*MAPT* mutation carriers) because there is no difference between asymptomatic and symptomatic *MAPT* mutation carriers. For MD, models include time from onset, group (symptomatic compared to asymptomatic *MAPT* mutation carriers) and interaction between time from onset and group.
Key: FA, fractional anisotropy; MAPT, microtubule-associated protein tau; MD, mean diffusivity; WM, white matter.

WM is present as early as the asymptomatic stage in *MAPT* mutation carriers; 2) the WM degeneration extends to the limbic tracts and the frontotemporal lobe WM in the symptomatic stage; 3) higher MD and lower FA in the entorhinal WM are associated with the proximity to the estimated and actual age of symptom onset; and 4) longitudinal increase of MD in the entorhinal WM accelerates with aging in *MAPT* mutation carriers compared with noncarriers.

The WM alterations on DTI can be linked to a variety of degenerative changes in the WM of *MAPT* mutation carriers. Progressive accumulation of hyperphosphorylated tau in neurons and glia caused by the *MAPT* mutation can impair the neuronal and axonal transport (Coleman, 2005; McAleese et al., 2017), and initiate a degenerative loss of axons and associated demyelination in FTLD (Adalbert et al., 2018). Furthermore, WM tau pathology were also observed in postmortem studies of *MAPT* mutation carriers (Sima et al., 1996), sporadic FTLD patients (Kovacs et al., 2008; Larsson et al., 2000), and animals expressing mutant tau (Gotz et al., 2001; Lin et al., 2003), even in the asymptomatic stage (Ling et al., 2016), indicating that WM degeneration occurs early and is a significant component of pathophysiology in *MAPT* mutation carriers.

In the present study, DTI findings in asymptomatic *MAPT* mutation carriers compared with noncarriers revealed higher MD in the entorhinal WM, which harbors the perforant pathway connecting the hippocampus and the entorhinal cortex. This early entorhinal WM involvement is concordant with the pattern of gray matter atrophy predominantly involving anteromedial temporal lobe in *MAPT* mutation carriers (Rohrer et al., 2015) and FTD patients (Fumagalli et al., 2018; Whitwell and Josephs, 2012). Entorhinal cortex is affected heavily with the tau pathology and subsequent atrophy, with a volume loss of about 28% in FTD patients compared with controls (Laakso et al., 2000). However, it is not yet clear if the entorhinal WM diffusion abnormalities are due to the Wallerian degeneration secondary to the cortical tau pathology or to the tau pathology observed in the WM. Pathologic correlation would be needed to determine the underlying pathophysiology of these WM changes in *MAPT* mutation carriers.

Previous cross-sectional studies have demonstrated reduced FA and increased diffusivity in bilateral uncinate fasciculus in asymptomatic *MAPT* mutation carriers (Dopper et al., 2014; Jiskoot et al., 2018). Furthermore, lower FA in uncinate fasciculus and other WM tracts were present 2 years before symptom onset in converters with *MAPT* and *GRN* mutations, whereas no difference in FA was found between asymptomatic *MAPT* mutation carriers who remained asymptomatic and noncarriers (Jiskoot et al., 2019). In the present study, we found diffusivity changes in the uncinate fasciculus only in symptomatic *MAPT* mutation carriers, while we did not find an alteration in diffusivity in the asymptomatic *MAPT* mutation carriers in this tract. On the other hand, MD was higher in the entorhinal WM in asymptomatic *MAPT* mutation carriers. This discrepancy may be related with region specific involvement at the different time windows during the disease process. It is possible that uncinate fasciculus may be involved right before conversion to symptomatic disease as demonstrated by Jiskoot et al., and many of the asymptomatic *MAPT* mutation carriers we studied may not have reached that stage. However, our findings in symptomatic *MAPT* mutation carriers demonstrate that uncinate fasciculus is involved at later stages.

The DTI findings in symptomatic *MAPT* mutation carriers compared with noncarriers revealed a pattern of increased MD and reduced FA primarily involving the WM connections of the limbic system network. Except for the entorhinal WM, increased MD was also observed in the fornix, which primarily carries the efferent projections from neurons of the hippocampus and from the subiculum to the subcortical gray matter and back; the uncinate fasciculus, which connects the anterior temporal lobe with the inferior frontal gyrus and the base of the frontal lobe; the cingulum tract, which carries hippocampal projections to the medial parietal lobe; the corpus callosum, which is the major commissure integrating the 2 hemispheres; the inferior fronto-occipital fasciculus, which connects the frontal and occipital lobes with some branches also terminating in the parietal and temporal lobes. This pattern of DTI alterations involving the limbic pathways connecting the anterio-medial temporal lobe to the subcortical gray matter, from temporal lobe to basal portion of frontal lobe and from frontal lobe to occipital lobe, is consistent with most of the DTI studies in patients with FTLD (Bertrand et al., 2018; Dopper et al., 2014; Elahi et al., 2017; Frings et al., 2014; Kassubek et al., 2018; Mahoney et al., 2015; Pievani et al., 2014; Whitwell et al., 2010).

Table 3
Annualized change of FA and MD in entorhinal WM from mixed-effects models (noncarrier as the reference group)

	FA		MD	
	Est (95% CI)	*p*	Est (95% CI)	*p*
Intercept	0.22 (0.16, 0.28)	<0.001	862 (579, 1146)	<0.001
Age at DTI scan	−0.0008 (−0.002, 0.0004)	0.17	0.50 (−3.34, 4.34)	0.80
Carrier	0.03 (−0.05, 0.12)	0.40	−433 (−724, −143)	0.006
Carrier × age at DTI scan	−0.002 (−0.003, 0.0001)	0.06	13.3 (7.50, 19.2)	<0.001

Models include age at DTI scans, combined *MAPT* mutation carriers group, and interaction between age and group, also accounting for family mutation.
Key: DTI, diffusion tensor image; FA, fractional anisotropy; *MAPT*, microtubule-associated protein tau; MD, mean diffusivity; WM, white matter.

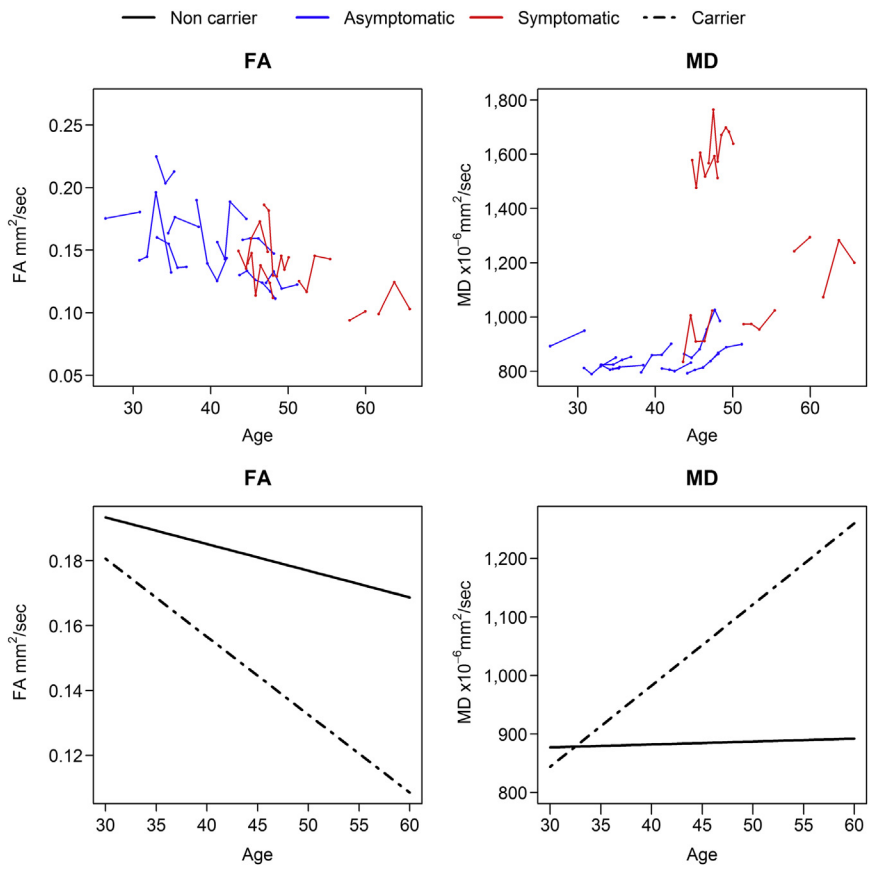

Fig. 3. FA and MD values plotted against age at MRI. Data points for individual participants are shown in the top panel with asymptomatic (blue line) and symptomatic (red line) *MAPT* mutation carriers. The dash line in lower panel represents the average FA and MD value for all *MAPT* mutation carriers, the solid line shows the average FA and MD value for noncarriers. Abbreviations: FA, fractional anisotropy; *MAPT*, microtubule-associated protein tau; MD, mean diffusivity. (For interpretation of the references to color in this figure legend, the reader is referred to the Web version of this article.)

We found an association between the entorhinal WM diffusion abnormalities and the proximity to symptom onset, characterized by decreasing FA and increasing MD as the participants approached the estimated age of onset that continued with a similar trend after passing the actual age of onset in the symptomatic group. Furthermore, with a median 4 years of follow-up, our longitudinal data provided information on annualized rates of change in DTI metrics, indicating that the annualized rates of increase in entorhinal WM MD in *MAPT* mutation carriers was faster than noncarriers. These findings demonstrated that the loss of WM integrity related to neurodegeneration occurred years before symptom onset and progressed over time in *MAPT* mutation carriers. A similar pattern of diffusion abnormality was reported in converters with *MAPT* and *GRN* mutations, demonstrating longitudinal decline of FA in uncinate fasciculus, genu and posterior corpus callosum, forceps minor, and superior longitudinal fasciculus (Jiskoot et al., 2019). Increasing MD and decreasing FA were also found in animal models of tauP301L mutations, along with the WM pathology. Increased diffusivity and lower FA were detected in the WM during the early stages preceding severe tauopathy, and got worse with a "disorganized" pattern of myelinated fiber arrangement with enlarged interaxonal spaces in the later stage (Jackson et al., 2018; Sahara et al., 2014).

The association of entorhinal MD with proximity to symptom onset was mainly driven by the symptomatic *MAPT* mutation carriers. A possible explanation is that entorhinal WM integrity was already impaired before symptom onset, but accelerated after clinical symptom onset. This is supported by our cross-sectional findings of higher MD in the entorhinal WM of asymptomatic *MAPT* mutation carriers compared with noncarriers. The

Table 4
Annual change in entorhinal WM (combined left/right) FA, and MD from mixed-effects models (noncarrier as the reference group)

	FA		MD	
	Est (95% CI)	*p*	Est (95% CI)	*p*
Intercept	0.22 (0.16, 0.28)	<0.001	887 (628, 1145)	<0.001
Age at DTI scan	−0.0008 (−0.002, 0.0004)	0.19	0.28 (−2.82, 3.39)	0.86
Asymptomatic	0.05 (−0.06, 0.15)	0.34	−104 (−367, 159)	0.42
Symptomatic	0.04 (−0.10, 0.17)	0.56	−722 (−1188, −256)	0.004
Asymptomatic × age at DTI scan	−0.002 (−0.004, 0.0002)	0.08	4.17 (−2.01, 10.4)	0.18
Symptomatic × age at DTI scan	−0.002 (−0.004, 0.0009)	0.21	18.8 (10.4, 27.1)	<0.001

Models include age at DTI scans, group, and interaction between age and group, also accounting for family mutation.
Key: DTI, diffusion tensor image; FA, fractional anisotropy; MD, mean diffusivity; WM, white matter.

accelerated increase of entorhinal MD was also noted in our 2 asymptomatic *MAPT* mutation carriers after they progressed to the symptomatic stage (Fig. 3).

MD was more sensitive than FA in detecting the longitudinal diffusion abnormalities in the asymptomatic and symptomatic stages, correlating with the disease progression in *MAPT* mutation carriers as they aged. These differences may in part be explained by variations in underlying pathological findings with disease progression. Elevation of MD in the asymptomatic stage and accelerating during the symptomatic stage may be related to the astrogliosis, laminar spongiosis (Sima et al., 1996) and microvacuolization (Mann et al., 1993) that would lead to an increase in free water in the extracellular space observed in *MAPT* mutation carriers during early stages of pathologic involvement. On the other hand, the consistent decline in FA may be due to a gradual loss of WM organization because of deafferentation in the projections from the ventral frontal and temporal lobe throughout disease progression, which may be linked to the neurodegenerative changes in the gray matter. FA could also be influenced by crossing fibers more than MD, which may have limited the sensitivity of FA to detect subtle WM degeneration (Jeurissen et al., 2013).

In our longitudinal cohort, we observed that 3 symptomatic carriers of the V337M *MAPT* mutation, from the same family, with disease duration up to 31 years had relatively lower MD values in entorhinal WM than symptomatic carriers of the S305N *MAPT* mutation with even shorter disease duration. Interestingly, the unusually delayed symptom onset and long duration was reported in another FTLD family with V337M mutation (Domoto-Reilly et al., 2017). Further studies are needed to fully characterize the WM abnormality and heterogeneous clinical presentation across different mutation types.

Limitations of our study include a small sample size and the unbalanced representation of *MAPT* families in carrier and noncarrier groups. Larger cohorts of asymptomatic *MAPT* mutation carriers are needed to longitudinally follow and establish the patterns of WM diffusion changes in specific tracts. Furthermore, the right hemispheric WM tracts had higher MD than the left but no difference in FA values in *MAPT* mutation carriers. Whether this asymmetry observed in this sample is generalizable to other samples need to be clarified in larger data sets. In addition, DTI remains an indirect measure of WM integrity. Although different DTI metrics may reflect different processes, linking them to specific pathologies remains challenging. Further studies are needed to characterize and compare the trajectory of change across different FTLD mutations, such as *GRN* and *C9orf72* mutations. Multishell DTI that enable measurements of neurite orientation dispersion and density imaging (Zhang et al., 2012) and multitissue constrained spherical deconvolution (Jeurissen et al., 2014) may address more specific characterization of tissue microstructure in *MAPT* mutation carriers than conventional DTI in future studies. Because heterogeneity was a common feature in symptom onset across different *MAPT* mutations/families and within the same family, future studies by tracking the trajectory of DTI alteration in *MAPT* mutation carriers with respect to the actual time of symptom onset during a longitudinal evaluation would provide more information.

5. Conclusions

In summary, we have demonstrated that DTI measures of WM microstructure appear sensitive to the earliest entorhinal WM changes in asymptomatic *MAPT* mutation carriers, which propagate to the limbic connections and temporofrontal projections in symptomatic *MAPT* mutation carriers. The DTI metrics in the entorhinal WM were also associated with the proximity to symptom onset and the disease progression. Our cross-sectional and longitudinal data showed a potential clinical utility for DTI to track neurodegenerative disease progression for *MAPT* mutation carriers in clinical trials. Future work is needed to confirm the sensitivity and reliability of DTI measurement in individual subjects.

Disclosure

The authors have no actual or potential conflicts of interest.

Acknowledgements

The authors extend our appreciation to Drs. John Hsiao and Dallas Anderson from the National Institute on Aging, Dr. Marg Sutherland from the National Institute of Neurological Disorders and Stroke, the staff of all centers, and particularly to our patients and their families for their participation in this protocol.

This work is supported by the National Institutes of Health (NIH) grants U01 AG045390, U54 NS092089, U24 AG021886, U01 AG016976 and R01 AG 40042.

Appendix A. Supplementary data

Supplementary data to this article can be found online at https://doi.org/10.1016/j.neurobiolaging.2019.08.011.

References

Adalbert, R., Milde, S., Durrant, C., Ando, K., Stygelbout, V., Yilmaz, Z., Gould, S., Brion, J.P., Coleman, M.P., 2018. Interaction between a MAPT variant causing frontotemporal dementia and mutant APP affects axonal transport. Neurobiol. Aging 68, 68–75.

Avants, B.B., Tustison, N.J., Song, G., Cook, P.A., Klein, A., Gee, J.C., 2011. A reproducible evaluation of ANTs similarity metric performance in brain image registration. Neuroimage 54, 2033–2044.

Bang, J., Spina, S., Miller, B.L., 2015. Frontotemporal dementia. Lancet 386, 1672–1682.

Bendlin, B.B., Carlsson, C.M., Johnson, S.C., Zetterberg, H., Blennow, K., Willette, A.A., Okonkwo, O.C., Sodhi, A., Ries, M.L., Birdsill, A.C., Alexander, A.L., Rowley, H.A., Puglielli, L., Asthana, S., Sager, M.A., 2012. CSF T-Tau/Abeta42 predicts white matter microstructure in healthy adults at risk for Alzheimer's disease. PLoS One 7, e37720.

Bertrand, A., Wen, J., Rinaldi, D., Houot, M., Sayah, S., Camuzat, A., Fournier, C., Fontanella, S., Routier, A., Couratier, P., Pasquier, F., Habert, M.O., Hannequin, D., Martinaud, O., Caroppo, P., Levy, R., Dubois, B., Brice, A., Durrleman, S., Colliot, O., Le Ber, I., Predict to Prevent Frontotemporal Lobar, D., Amyotrophic Lateral Sclerosis Study, G., 2018. Early cognitive, structural, and microstructural changes in presymptomatic C9orf72 carriers younger than 40 years. JAMA Neurol. 75, 236–245.

Bunker, J.M., Kamath, K., Wilson, L., Jordan, M.A., Feinstein, S.C., 2006. FTDP-17 mutations compromise the ability of tau to regulate microtubule dynamics in cells. J. Biol. Chem. 281, 11856–11863.

Cash, D.M., Bocchetta, M., Thomas, D.L., Dick, K.M., van Swieten, J.C., Borroni, B., Galimberti, D., Masellis, M., Tartaglia, M.C., Rowe, J.B., Graff, C., Tagliavini, F., Frisoni, G.B., Laforce Jr., R., Finger, E., de Mendonca, A., Sorbi, S., Rossor, M.N., Ourselin, S., Rohrer, J.D., Genetic Ftd Initiative, G., 2018. Patterns of gray matter atrophy in genetic frontotemporal dementia: results from the GENFI study. Neurobiol. Aging 62, 191–196.

Coleman, M., 2005. Axon degeneration mechanisms: commonality amid diversity. Nat. Rev. Neurosci. 6, 889–898.

Domoto-Reilly, K., Davis, M.Y., Keene, C.D., Bird, T.D., 2017. Unusually long duration and delayed penetrance in a family with FTD and mutation in MAPT (V337M). Am. J. Med. Genet. B Neuropsychiatr. Genet. 174, 70–74.

Dopper, E.G., Rombouts, S.A., Jiskoot, L.C., den Heijer, T., de Graaf, J.R., de Koning, I., Hammerschlag, A.R., Seelaar, H., Seeley, W.W., Veer, I.M., van Buchem, M.A., Rizzu, P., van Swieten, J.C., 2014. Structural and functional brain connectivity in presymptomatic familial frontotemporal dementia. Neurology 83, e19–e26.

Elahi, F.M., Marx, G., Cobigo, Y., Staffaroni, A.M., Kornak, J., Tosun, D., Boxer, A.L., Kramer, J.H., Miller, B.L., Rosen, H.J., 2017. Longitudinal white matter change in frontotemporal dementia subtypes and sporadic late onset Alzheimer's disease. Neuroimage Clin. 16, 595–603.

Frings, L., Yew, B., Flanagan, E., Lam, B.Y., Hull, M., Huppertz, H.J., Hodges, J.R., Hornberger, M., 2014. Longitudinal grey and white matter changes in frontotemporal dementia and Alzheimer's disease. PLoS One 9, e90814.

Fumagalli, G.G., Basilico, P., Arighi, A., Bocchetta, M., Dick, K.M., Cash, D.M., Harding, S., Mercurio, M., Fenoglio, C., Pietroboni, A.M., Ghezzi, L., van Swieten, J., Borroni, B., de Mendonca, A., Masellis, M., Tartaglia, M.C., Rowe, J.B.,

Graff, C., Tagliavini, F., Frisoni, G.B., Laforce Jr., R., Finger, E., Sorbi, S., Scarpini, E., Rohrer, J.D., Galimberti, D., Genetic, F.T.D.I., 2018. Distinct patterns of brain atrophy in Genetic Frontotemporal Dementia Initiative (GENFI) cohort revealed by visual rating scales. Alzheimers Res. Ther. 10, 46.

Garyfallidis, E., Brett, M., Amirbekian, B., Rokem, A., van der Walt, S., Descoteaux, M., Nimmo-Smith, I., Dipy, C., 2014. Dipy, a library for the analysis of diffusion MRI data. Front Neuroinform. 8, 8.

Gotz, J., Chen, F., Barmettler, R., Nitsch, R.M., 2001. Tau filament formation in transgenic mice expressing P301L tau. J. Biol. Chem. 276, 529–534.

Hutton, M., Lendon, C.L., Rizzu, P., Baker, M., Froelich, S., Houlden, H., Pickering-Brown, S., Chakraverty, S., Isaacs, A., Grover, A., Hackett, J., Adamson, J., Lincoln, S., Dickson, D., Davies, P., Petersen, R.C., Stevens, M., de Graaff, E., Wauters, E., van Baren, J., Hillebrand, M., Joosse, M., Kwon, J.M., Nowotny, P., Che, L.K., Norton, J., Morris, J.C., Reed, L.A., Trojanowski, J., Basun, H., Lannfelt, L., Neystat, M., Fahn, S., Dark, F., Tannenberg, T., Dodd, P.R., Hayward, N., Kwok, J.B., Schofield, P.R., Andreadis, A., Snowden, J., Craufurd, D., Neary, D., Owen, F., Oostra, B.A., Hardy, J., Goate, A., van Swieten, J., Mann, D., Lynch, T., Heutink, P., 1998. Association of missense and 5'-splice-site mutations in tau with the inherited dementia FTDP-17. Nature 393, 702–705.

Ingram, E.M., Spillantini, M.G., 2002. Tau gene mutations: dissecting the pathogenesis of FTDP-17. Trends Mol. Med. 8, 555–562.

Jackson, J., Bianco, G., Rosa, A.O., Cowan, K., Bond, P., Anichtchik, O., Fern, R., 2018. White matter tauopathy: transient functional loss and novel myelin remodeling. Glia 66, 813–827.

Jeurissen, B., Leemans, A., Tournier, J.D., Jones, D.K., Sijbers, J., 2013. Investigating the prevalence of complex fiber configurations in white matter tissue with diffusion magnetic resonance imaging. Hum. Brain Mapp. 34, 2747–2766.

Jeurissen, B., Tournier, J.D., Dhollander, T., Connelly, A., Sijbers, J., 2014. Multi-tissue constrained spherical deconvolution for improved analysis of multi-shell diffusion MRI data. Neuroimage 103, 411–426.

Jiskoot, L.C., Bocchetta, M., Nicholas, J.M., Cash, D.M., Thomas, D., Modat, M., Ourselin, S., Rombouts, S., Dopper, E.G.P., Meeter, L.H., Panman, J.L., van Minkelen, R., van der Ende, E.L., Donker Kaat, L., Pijnenburg, Y.A.L., Borroni, B., Galimberti, D., Masellis, M., Tartaglia, M.C., Rowe, J., Graff, C., Tagliavini, F., Frisoni, G.B., Laforce Jr., R., Finger, E., de Mendonca, A., Sorbi, S., , Genetic Frontotemporal dementia, I., Papma, J.M., van Swieten, J.C., Rohrer, J.D., 2018. Presymptomatic white matter integrity loss in familial frontotemporal dementia in the GENFI cohort: a cross-sectional diffusion tensor imaging study. Ann. Clin. Transl. Neurol. 5, 1025–1036.

Jiskoot, L.C., Panman, J.L., Meeter, L.H., Dopper, E.G.P., Donker Kaat, L., Franzen, S., van der Ende, E.L., van Minkelen, R., Rombouts, S., Papma, J.M., van Swieten, J.C., 2019. Longitudinal multimodal MRI as prognostic and diagnostic biomarker in presymptomatic familial frontotemporal dementia. Brain 142, 193–208.

Kantarci, K., Boeve, B.F., Wszolek, Z.K., Rademakers, R., Whitwell, J.L., Baker, M.C., Senjem, M.L., Samikoglu, A.R., Knopman, D.S., Petersen, R.C., Jack Jr., C.R., 2010. MRS in presymptomatic MAPT mutation carriers: a potential biomarker for tau-mediated pathology. Neurology 75, 771–778.

Kantarci, K., Murray, M.E., Schwarz, C.G., Reid, R.I., Przybelski, S.A., Lesnick, T., Zuk, S.M., Raman, M.R., Senjem, M.L., Gunter, J.L., Boeve, B.F., Knopman, D.S., Parisi, J.E., Petersen, R.C., Jack Jr., C.R., Dickson, D.W., 2017. White-matter integrity on DTI and the pathologic staging of Alzheimer's disease. Neurobiol. Aging 56, 172–179.

Kassubek, J., Muller, H.P., Del Tredici, K., Hornberger, M., Schroeter, M.L., Muller, K., Anderl-Straub, S., Uttner, I., Grossman, M., Braak, H., Hodges, J.R., Piguet, O., Otto, M., Ludolph, A.C., 2018. Longitudinal diffusion tensor imaging resembles patterns of pathology progression in behavioral variant frontotemporal dementia (bvFTD). Front Aging Neurosci. 10, 47.

Knopman, D.S., Kramer, J.H., Boeve, B.F., Caselli, R.J., Graff-Radford, N.R., Mendez, M.F., Miller, B.L., Mercaldo, N., 2008. Development of methodology for conducting clinical trials in frontotemporal lobar degeneration. Brain 131 (Pt 11), 2957–2968.

Kovacs, G.G., Majtenyi, K., Spina, S., Murrell, J.R., Gelpi, E., Hoftberger, R., Fraser, G., Crowther, R.A., Goedert, M., Budka, H., Ghetti, B., 2008. White matter tauopathy with globular glial inclusions: a distinct sporadic frontotemporal lobar degeneration. J. Neuropathol. Exp. Neurol. 67, 963–975.

Laakso, M.P., Frisoni, G.B., Kononen, M., Mikkonen, M., Beltramello, A., Geroldi, C., Bianchetti, A., Trabucchi, M., Soininen, H., Aronen, H.J., 2000. Hippocampus and entorhinal cortex in frontotemporal dementia and Alzheimer's disease: a morphometric MRI study. Biol. Psychiatry 47, 1056–1063.

Larsson, E., Passant, U., Sundgren, P.C., Englund, E., Brun, A., Lindgren, A., Gustafson, L., 2000. Magnetic resonance imaging and histopathology in dementia, clinically of frontotemporal type. Dement. Geriatr. Cogn. Disord. 11, 123–134.

Lin, W.L., Lewis, J., Yen, S.H., Hutton, M., Dickson, D.W., 2003. Filamentous tau in oligodendrocytes and astrocytes of transgenic mice expressing the human tau isoform with the P301L mutation. Am. J. Pathol. 162, 213–218.

Ling, H., Kovacs, G.G., Vonsattel, J.P., Davey, K., Mok, K.Y., Hardy, J., Morris, H.R., Warner, T.T., Holton, J.L., Revesz, T., 2016. Astrogliopathy predominates the earliest stage of corticobasal degeneration pathology. Brain 139 (Pt 12), 3237–3252.

Mahoney, C.J., Simpson, I.J., Nicholas, J.M., Fletcher, P.D., Downey, L.E., Golden, H.L., Clark, C.N., Schmitz, N., Rohrer, J.D., Schott, J.M., Zhang, H., Ourselin, S., Warren, J.D., Fox, N.C., 2015. Longitudinal diffusion tensor imaging in frontotemporal dementia. Ann. Neurol. 77, 33–46.

Mann, D.M., South, P.W., Snowden, J.S., Neary, D., 1993. Dementia of frontal lobe type: neuropathology and immunohistochemistry. J. Neurol. Neurosurg. Psychiatry 56, 605–614.

McAleese, K.E., Walker, L., Graham, S., Moya, E.L.J., Johnson, M., Erskine, D., Colloby, S.J., Dey, M., Martin-Ruiz, C., Taylor, J.P., Thomas, A.J., McKeith, I.G., De Carli, C., Attems, J., 2017. Parietal white matter lesions in Alzheimer's disease are associated with cortical neurodegenerative pathology, but not with small vessel disease. Acta Neuropathol. 134, 459–473.

Oishi, K., Zilles, K., Amunts, K., Faria, A., Jiang, H., Li, X., Akhter, K., Hua, K., Woods, R., Toga, A.W., Pike, G.B., Rosa-Neto, P., Evans, A., Zhang, J., Huang, H., Miller, M.I., van Zijl, P.C., Mazziotta, J., Mori, S., 2008. Human brain white matter atlas: identification and assignment of common anatomical structures in superficial white matter. Neuroimage 43, 447–457.

Panman, J.L., Jiskoot, L.C., Bouts, M., Meeter, L.H.H., van der Ende, E.L., Poos, J.M., Feis, R.A., Kievit, A.J.A., van Minkelen, R., Dopper, E.G.P., Rombouts, S., van Swieten, J.C., Papma, J.M., 2019. Gray and white matter changes in presymptomatic genetic frontotemporal dementia: a longitudinal MRI study. Neurobiol. Aging 76, 115–124.

Pievani, M., Paternico, D., Benussi, L., Binetti, G., Orlandini, A., Cobelli, M., Magnaldi, S., Ghidoni, R., Frisoni, G.B., 2014. Pattern of structural and functional brain abnormalities in asymptomatic granulin mutation carriers. Alzheimers Dement. 10 (5 Suppl), S354–S363.e1.

Rascovsky, K., Hodges, J.R., Knopman, D., Mendez, M.F., Kramer, J.H., Neuhaus, J., van Swieten, J.C., Seelaar, H., Dopper, E.G., Onyike, C.U., Hillis, A.E., Josephs, K.A., Boeve, B.F., Kertesz, A., Seeley, W.W., Rankin, K.P., Johnson, J.K., Gorno-Tempini, M.L., Rosen, H., Prioleau-Latham, C.E., Lee, A., Kipps, C.M., Lillo, P., Piguet, O., Rohrer, J.D., Rossor, M.N., Warren, J.D., Fox, N.C., Galasko, D., Salmon, D.P., Black, S.E., Mesulam, M., Weintraub, S., Dickerson, B.C., Diehl-Schmid, J., Pasquier, F., Deramecourt, V., Lebert, F., Pijnenburg, Y., Chow, T.W., Manes, F., Grafman, J., Cappa, S.F., Freedman, M., Grossman, M., Miller, B.L., 2011. Sensitivity of revised diagnostic criteria for the behavioural variant of frontotemporal dementia. Brain 134 (Pt 9), 2456–2477.

Reid, R.I., Nedelska, Z., Schwarz, C.G., Ward, C., Jack, C.R., 2018. Diffusion Specific Segmentation: Skull Stripping with Diffusion MRI Data Alone. Springer International Publishing, Cham, pp. 67–80.

Rohrer, J.D., Nicholas, J.M., Cash, D.M., van Swieten, J., Dopper, E., Jiskoot, L., van Minkelen, R., Rombouts, S.A., Cardoso, M.J., Clegg, S., Espak, M., Mead, S., Thomas, D.L., De Vita, E., Masellis, M., Black, S.E., Freedman, M., Keren, R., MacIntosh, B.J., Rogaeva, E., Tang-Wai, D., Tartaglia, M.C., Laforce Jr., R., Tagliavini, F., Tiraboschi, P., Redaelli, V., Prioni, S., Grisoli, M., Borroni, B., Padovani, A., Galimberti, D., Scarpini, E., Arighi, A., Fumagalli, G., Rowe, J.B., Coyle-Gilchrist, I., Graff, C., Fallstrom, M., Jelic, V., Stahlbom, A.K., Andersson, C., Thonberg, H., Lilius, L., Frisoni, G.B., Pievani, M., Bocchetta, M., Benussi, L., Ghidoni, R., Finger, E., Sorbi, S., Nacmias, B., Lombardi, G., Polito, C., Warren, J.D., Ourselin, S., Fox, N.C., Rossor, M.N., Binetti, G., 2015. Presymptomatic cognitive and neuroanatomical changes in genetic frontotemporal dementia in the Genetic Frontotemporal dementia Initiative (GENFI) study: a cross-sectional analysis. Lancet Neurol. 14, 253–262.

Rohrer, J.D., Warren, J.D., 2011. Phenotypic signatures of genetic frontotemporal dementia. Curr. Opin. Neurol. 24, 542–549.

Sahara, N., Perez, P.D., Lin, W.L., Dickson, D.W., Ren, Y., Zeng, H., Lewis, J., Febo, M., 2014. Age-related decline in white matter integrity in a mouse model of tauopathy: an in vivo diffusion tensor magnetic resonance imaging study. Neurobiol. Aging 35, 1364–1374.

Sima, A.A., Defendini, R., Keohane, C., D'Amato, C., Foster, N.L., Parchi, P., Gambetti, P., Lynch, T., Wilhelmsen, K.C., 1996. The neuropathology of chromosome 17-linked dementia. Ann. Neurol. 39, 734–743.

Spillantini, M.G., Murrell, J.R., Goedert, M., Farlow, M.R., Klug, A., Ghetti, B., 1998. Mutation in the tau gene in familial multiple system tauopathy with presenile dementia. Proc. Natl. Acad. Sci. U. S. A. 95, 7737–7741.

Whitwell, J.L., Avula, R., Senjem, M.L., Kantarci, K., Weigand, S.D., Samikoglu, A., Edmonson, H.A., Vemuri, P., Knopman, D.S., Boeve, B.F., Petersen, R.C., Josephs, K.A., Jack Jr., C.R., 2010. Gray and white matter water diffusion in the syndromic variants of frontotemporal dementia. Neurology 74, 1279–1287.

Whitwell, J.L., Josephs, K.A., 2012. Neuroimaging in frontotemporal lobar degeneration–predicting molecular pathology. Nat. Rev. Neurol. 8, 131–142.

Zhang, H., Schneider, T., Wheeler-Kingshott, C.A., Alexander, D.C., 2012. NODDI: practical in vivo neurite orientation dispersion and density imaging of the human brain. Neuroimage 61, 1000–1016.